acoustics

Article

Modelling of Shell Trumpet Overtones and Acoustics of Helicoidal Geometries

Marcel-André Ramírez-Trocherie [1,2,*], Pablo Padilla [3], Francisca Zalaquett [4] and Martín Salinas-Vázquez [1]

[1] Instituto de Ingeniería, Universidad Nacional Autónoma de México, Circuito Escolar, Ciudad Universitaria, CDMX, Mexico City CP 04510, Mexico
[2] Colegio de Ciencias y Humanidades (CCH) Plantel Sur, Universidad Nacional Autónoma de México, Cataratas y Llanura S/N, Jardines del Pedregal, Coyoacán, CDMX, Mexico City CP 04500, Mexico
[3] Instituto de Investigaciones en Matemáticas Aplicadas y Sistemas, Universidad Nacional Autónoma de México, Circuito Mario de la Cueva, Ciudad Universitaria, CDMX, Mexico City CP 04510, Mexico
[4] Centro de Estudios Mayas en Instituto de Investigaciones Filológicas, Universidad Nacional Autónoma de México, Circuito Mario de la Cueva, Ciudad Universitaria, CDMX, Mexico City CP 04510, Mexico; franciscazalaquettr@gmail.com
* Correspondence: marcel_andre.ramirez@cch.unam.mx

Abstract

In this work, the propagation of acoustic waves in shell trumpets is explored, and the overtones generated by them are studied. We consider different shell geometries, for which their particular morphology is taken into account. This impacts the fundamental frequencies as well as the overtones. An analytical model based on differential equations is developed to predict these overtones and compared with real recordings of some shell trumpets belonging to several collections in Mexico (experimental results). As a consequence, the notes of archaeological shells that cannot be played due to their physical damage are estimated.

Keywords: acoustic wave; Mesoamerican seashell; helicoidal geometry; Webster's horn; acoustics of musical instruments

1. Introduction

In this paper, we present results on the study of aerophones made from marine shells (gastropods). The vibrating mass inside the shell is a column of air, shaped with a helicoidal twist. The pre-Hispanic Maya materials analyzed have been dated to the Late Classic period (600–900 A.D.) and come from the Jaina archaeological site, Campeche, Mexico (shell coded 10-34283, Pleuroploca gigantea), from a surface collection at the Plazuelas archaeological site, Guanajuato (shells 10-412970, 10-412971, Pleuroploca gigantea) and from the National Museum of Anthropology (shell coded 10-621154, undetermined species).

Also, two ceramic shell-like pieces (codes 10-223524 and 10-393463) were obtained from the Maya Room of the National Museum of Anthropology, Mexico.

Conches, both shell and ceramic, have been found in many archaeological excavations at a variety of Maya settlements, either as sound instruments, representations in stone reliefs or painted on polychrome vessels, among others.

The acoustic description of the conches has biological, archaeological, and organological approaches since multiple records of instrument shells dating back to the Paleolithic period are studied [1] and since multiple conches are intentionally damaged in ritualistic processes to release the spirit of the object at the end of its use, leaving them acoustically inoperative [2].

Academic Editors: Brian FG Katz and Francesco Aletta

Received: 10 February 2026
Revised: 7 March 2026
Accepted: 20 March 2026
Published: 1 April 2026

The development of the shell (that is made of calcium carbonate) begins during the larval period of the gastropod. The resulting shell takes the same shape as the torsion of the larva's body: a cone with spiral walls molded helicoidally [3]. Inside the structure, the succession and contact of the spiral walls form a tubular conical framework, called the "columella," which houses the visceral mass [4].

The acoustical characterization of spaces with helicoidal geometry is important both from a theoretical point of view and for its applications. From an analytical perspective, these domains offer the possibility of exploring the effects of curvature on wave propagation, as well as nonlinear phenomena of geometric origin [5]. In [6] studies on the human cochlea with medical applications were performed, demonstrating the importance of the study of acoustics in this type of morphology. Optimization of space and energy in spiral-shaped car horns was presented in [7]. In [8] a study in ANSYS 12.0 was conducted to observe sound pressure and main acoustic harmonics inside a snail-type horn. In this analysis the authors consider a nonviscous fluid, and the influence of the wall material on the characteristic timbre of the trumpet is not taken into account. Also, ref. [9] studied seashells of the type *Xancus pyrum* as acoustical instruments from a theoretical lip–instrument interaction, coupling the acoustic impedance of the shell with vibration of the lips. Similar studies on shells [10] have been done only numerically, without obtaining analytical solutions due to their complexity.

In this paper, the behavior of acoustic waves produced by trumpets made of sea snails is explored by means of asymptotic methods, as well as by comparing the models with recordings of original Mesoamerican trumpets. These models will allow us to predict the overtones of Mesoamerican trumpets that for various reasons cannot be played (fragility or/and previous damage, among others). This study is also useful for developing predictive models to assess and determine the sound ranges of archaeological fragments, which will help as a guide for conducting acoustic restorations of these materials, which have great cultural value.

2. Geometry of a Snail Seashell

The geometry of a snail seashell has multiple complexities, since the growth of these animals resembles a spiral. This has been studied by Archimedes (whom a special type of spiral has been named after), and Fermat, among others. In the case of seashells, the underlying curve is a helix (Figure 1), since it is a curve in three-dimensional space.

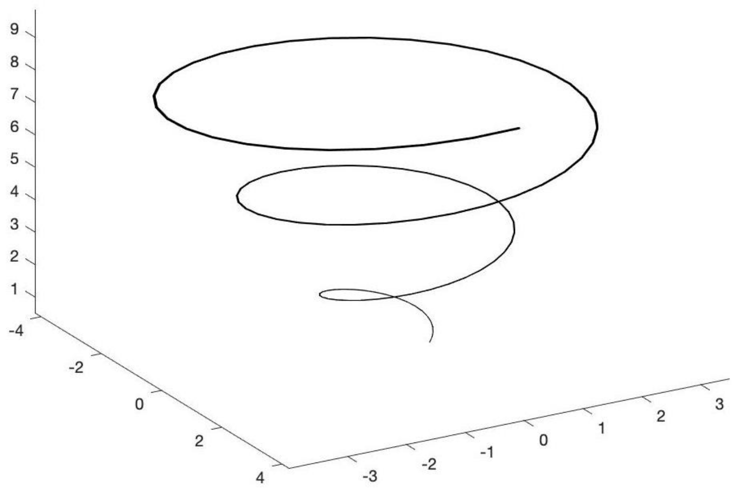

Figure 1. Generating curve (helix).

Due to the geometry of the seashell that grows as an Archimedean spiral [11] we use a helicoidal trumpet that we have chosen to generate an adapted helicoidal coordinate system, that allows us to model the surface with ducts and boundary conditions.

As a first step, a helix will be constructed since it will be used as the basis to generate the helicoidal coordinate system. We will focus on the following family of curves, parametrically described in a Cartesian coordinate system:

$$\begin{aligned} x &= \big(f(\theta)\big)\cos(\theta) \\ y &= \big(f(\theta)\big)\sin(\theta) \\ z &= M(\theta), \end{aligned} \tag{1}$$

where $f(\theta)$ is the function which represents the radius of the two-dimensional projection on the XY plane, $M(\theta)$ is the function that indicates the growth of the curve in the direction of z, and $f(0)$ and $M(0)$ are the initial radius and the initial plane z respectively. Also, we remark that θ is an angular parameter. It should be noted that there is a good agreement between this family of curves and the biological specimens [12].

At each point of the above-mentioned helix (Equation (1)), a type of Frenet–Serret trihedral coordinate system can be generated in polar coordinates as in [13,14]. Standard equations (Equation (8)) in [14] were extended to the case of a helical pipe flow by [15] who had previously also studied the effect of torsion in [16]. This is adequate since with a suitable coordinate system the internal surface of the seashell can be described. It is also noted that in [16] similar equations were used in later years to study incompressible flows [17], while the model in the present work applies to a compressible flow.

Based on the ideas of the mobile trihedron by Frenet–Serret, the curve is reparameterized as suggested in [18] in terms of the arc length s.

The arc length can be obtained as follows:

$$\begin{aligned} \frac{dx}{d\theta} &= -f(\theta)\sin(\theta) + \cos(\theta)f'(\theta) \\ \frac{dy}{d\theta} &= f(\theta)\cos(\theta) + \sin(\theta)f'(\theta) \\ \frac{dz}{d\theta} &= M'(\theta) \end{aligned} \tag{2}$$

$$ds = \sqrt{f(\theta)^2 + f'(\theta)^2 + M'(\theta)^2} \quad d\theta \tag{3}$$

$$s = \int_{\theta_0}^{\theta} \sqrt{f(\vartheta)^2 + f'(\vartheta)^2 + M'(\vartheta)^2} \quad d\vartheta. \tag{4}$$

It can be observed that the integrand is a monotone increasing function if $f(\theta)$ and $M(\theta)$ are monotone increasing functions, so the function $s = S(\theta)$ is increasing. Therefore there exists an invertible function $\theta = S^{-1}(s)$. In the case of a seashell, this occurs because their shell always grows volumetrically and it never happens that it reduces its size. If the function exists, and is defined for the compact support of the parameter of the curve, it can be reparametrized by means of s.

The Frenet–Serret trihedron is an orthonormal coordinate system determined by $\vec{T}(s)$, $\vec{N}(s)$ and $\vec{B}(s)$ (with $\vec{T}(s)$, $\vec{N}(s)$ and $\vec{B}(s)$ respectively being the tangent vector, the normal vector and the binormal vector) as the basis of the new coordinate system.

The chosen coordinate system is adapted to the curve that passes through the center of each of the circles that generate the trumpet surface. The system is generated by the tangent vector of the previously described curve (Equation (1)). We introduce polar coordinates on the plane generated by the normal and binormal vectors.

Our helicoidal system has coordinates s, r and α, being respectively arc length, internal radius of the pipe and internal angle of the pipe. Any vector described in terms of the new coordinate system is given by

$$\vec{R}(s,r,\alpha) = \vec{C}(s) + r\cos(\alpha+\phi(s))\vec{N}(s) + r\sin(\alpha+\phi(s))\vec{B}(s), \tag{5}$$

with

$$\phi(s) = -\int_{s_0}^{s} \tau(\xi)d\xi, \tag{6}$$

where $\tau(s)$ is the torsion of the curve $\vec{C}(s)$.

We obtain the differential length

$$\begin{aligned} d\vec{R} = {}& \big(1-\kappa r\cos(\alpha+\phi(s))\big)\vec{T}(s)ds \\ &+\big(\cos(\alpha+\phi(s))\vec{B}(s) - \sin(\alpha+\phi(s))\vec{N}(s)\big)dr \\ &-r\big(\cos(\alpha+\phi(s))\vec{N}(s) + \sin(\alpha+\phi(s))\vec{B}(s)\big)d\alpha. \end{aligned} \tag{7}$$

For computing the scale factors and the orthogonality of the system, the module of (Equation (7)) is computed:

$$d\vec{R}\cdot d\vec{R} = \big(1-\kappa r\cos(\alpha+\phi(s))\big)^2 ds^2 + dr^2 + r^2 d\alpha^2. \tag{8}$$

Since there are no crossed terms, it can be seen that the proposed system is orthogonal. Unlike the Frênet–Serret trihedron, space is described in terms of a polar coordinate system that moves along with a smooth curve.

Additionally, it can be observed that the scale factors are

$$h_s = 1-\kappa r\cos(\alpha+\phi(s)) \tag{9}$$

$$h_r = 1 \tag{10}$$

$$h_\alpha = r. \tag{11}$$

The surfaces generated by this coordinate system, which when intersected create a point, are as follows:

For constant r, a duct of a constant circular section follows the shape of the chosen curve.

For constant α, a half-plane is generated that follows the chosen curve.

For constant s, a plane perpendicular to the curve is generated at the point that coincides with the arc length.

Some examples of the type of surfaces that are generated from the family of helicoidal curves are illustrated in the figures: Figure 2 resembles the geometry of a sea shell, Figure 3 shows a Torus studied by Rienstra, and Figure 4 emulates the geometry of a French horn. We remark that these geometries can be useful in the study of other musical instruments.

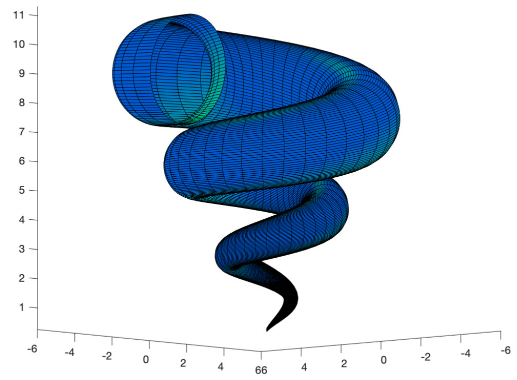

Figure 2. Helicoid.

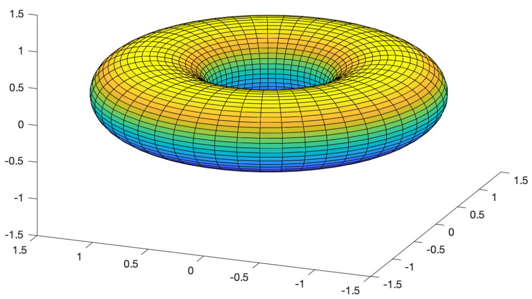

Figure 3. Torus; $M(\theta) = 0$ and $f(\theta)$ constant.

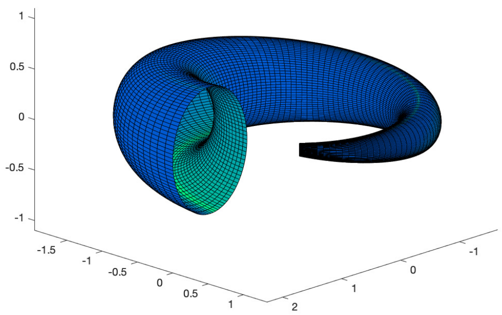

Figure 4. Helicoid at $M(\theta) = 0$.

The Cartesian equations for a special case of these surfaces considering a circular-cross-section pipe acquire the form

$$\begin{aligned} x &= \big(R_g(\theta) + r_t(\theta)\sin(\alpha)\big)\cos(\theta) \\ y &= \big(R_g(\theta) + r_t(\theta)\sin(\alpha)\big)\sin(\theta) \\ z &= r_t(\theta)\cos(\theta) + M(\theta), \end{aligned} \tag{12}$$

where $R_g(\theta)$ is the growth of the helix radius, $r_t(\theta)$ the radius of the pipe and $M(\theta)$ the growth of the planes where the surface is generated.

By having the scale factors, it is possible to describe differential operators in this new coordinate and orthogonal system.

The Laplacian for a scalar field that we use later is written as

$$\begin{aligned} \nabla^2\Phi = \frac{1}{h_r h_\alpha h_s}\bigg[&\frac{\partial}{\partial r}\left(\frac{h_\alpha h_s}{h_r}\frac{\partial\Phi}{\partial r}\right) + \frac{\partial}{\partial\alpha}\left(\frac{h_r h_s}{h_\alpha}\frac{\partial\Phi}{\partial\alpha}\right) \\ &+ \frac{\partial}{\partial s}\left(\frac{h_r h_\alpha}{h_s}\frac{\partial\Phi}{\partial s}\right)\bigg]. \end{aligned} \tag{13}$$

Replacing the scale factors:

$$\nabla^2\Phi = \frac{1}{rh_s}\frac{\partial}{\partial r}\left(rh_s\frac{\partial\Phi}{\partial r}\right) + \frac{1}{r^2h_s}\frac{\partial}{\partial\alpha}\left(h_s\frac{\partial\Phi}{\partial\alpha}\right) + \frac{1}{h_s}\frac{\partial}{\partial s}\left(\frac{1}{h_s}\frac{\partial\Phi}{\partial s}\right). \tag{14}$$

It should be noticed that the functional relationship of the scale factors does not allow the use of separation of variables.

3. Acoustic Approach

Webster [19] proposed a 1D simplification for ducts with variable area along one dimension by means of asymptotic expansions.

First, we start from the linear equation of acoustics. The model assumes low-frequency waves, which coincide with audible waves, and also assumes that the gradient of the wavefront is orthogonal to the cross section of the trumpet. In this work we will extend Webster's applications to snail seashell trumpets.

We use the standard wave equation for pressure [20]:

$$\frac{\partial^2\tilde{P}}{\partial t^2} = c_0^2\nabla^2\tilde{P}, \quad c_0^2 = \frac{RT}{M}, \tag{15}$$

where $\tilde{P}$ is the deviation of pressure from atmospheric pressure, and c_0 is the speed of sound in a gas (the constants that appear in its definition are to be determined experimentally).

Performing an analysis of orders of magnitude in the pressure as suggested by [20], it is found that $\tilde{P}$ is the deviation from the atmospheric pressure, varying several orders of magnitude from the atmospheric pressure, and c_0 is the speed of sound.

The Laplacian for the wave equation in the helicoidal coordinate system is

$$\nabla^2\tilde{P} = \frac{\partial^2\tilde{P}}{\partial r^2} + \frac{1}{r}\frac{\partial\tilde{P}}{\partial r} - \frac{\kappa\cos(\alpha+\phi)}{h_s}\frac{\partial\tilde{P}}{\partial r} + \frac{1}{r^2}\frac{\partial^2\tilde{P}}{\partial\alpha^2} + \frac{\kappa\sin(\alpha+\phi)}{rh_s}\frac{\partial\tilde{P}}{\partial\alpha} + \frac{1}{h_s}\frac{\partial}{\partial s}\left(\frac{1}{h_s}\frac{\partial\tilde{P}}{\partial s}\right). \tag{16}$$

We introduce the characteristic scales:

$$r = \varrho\tilde{r}, \quad s = \zeta L \quad \kappa = \varkappa\frac{1}{L}, \quad t = t^*\frac{L}{c_0}. \tag{17}$$

with

$$\mathcal{O}(\varrho) \sim 1, \quad \mathcal{O}(\zeta) \sim 1, \quad \mathcal{O}(\varkappa) \sim 1, \tag{18}$$

in order to write the wave equation in its dimensionless form.

The characteristic dimensions are $\tilde{r}$ (the maximum radius, coinciding with the bell of the trumpet), L (the travel length), c_0 (the speed of sound in air), κ (the curvature) and t (the time).

Substituting Equation (17) into the wave equation, we get

$$\frac{c^2}{c^2L^2}\frac{\partial^2\tilde{P}}{\partial t^{*2}} = \frac{1}{\tilde{r}^2}\frac{\partial^2\tilde{P}}{\partial\varrho^2} + \frac{1}{\tilde{r}^2\varrho}\frac{\partial\tilde{P}}{\partial\varrho} - \frac{\varkappa\cos(\alpha+\phi)}{L\tilde{r}h_s}\frac{\partial\tilde{P}}{\partial\varrho} + \frac{1}{\tilde{r}^2\varrho^2}\frac{\partial^2\tilde{P}}{\partial\alpha^2} + \frac{\varkappa\sin(\alpha+\phi)}{L\varrho\tilde{r}h_s}\frac{\partial\tilde{P}}{\partial\alpha} + \frac{1}{L^2h_s}\frac{\partial}{\partial\zeta}\left(\frac{1}{h_s}\frac{\partial\tilde{P}}{\partial\zeta}\right), + \tag{19}$$

with

$$h_s = 1 - \frac{\tilde{r}}{L}\varkappa\varrho\cos(\alpha+\phi). \tag{20}$$

Multiplying Equation (19) by $\tilde{r}^2$ and grouping in orders of $\varepsilon = \frac{\tilde{r}}{L}$,

$$\begin{aligned} &\frac{\partial^2\tilde{P}}{\partial\varrho^2} + \frac{1}{\varrho^2}\frac{\partial^2\tilde{P}}{\partial\alpha^2} + \frac{1}{\varrho}\frac{\partial\tilde{P}}{\partial\varrho} \\ +\varepsilon&\left(\frac{\varkappa\sin(\alpha+\phi)}{\varrho h_s}\frac{\partial\tilde{P}}{\partial\alpha} - \frac{\varkappa\cos(\alpha+\phi)}{h_s}\frac{\partial\tilde{P}}{\partial\varrho}\right) \\ +\varepsilon^2&\left(\frac{1}{h_s}\frac{\partial}{\partial\zeta}\left(\frac{1}{h_s}\frac{\partial\tilde{P}}{\partial\zeta}\right) - \frac{\partial^2\tilde{P}}{\partial t^{*2}}\right) = 0, \end{aligned} \tag{21}$$

where the radius of the bell is less than the total arc length of the helix

$$\varepsilon << 1. \tag{22}$$

We work in the same way with the boundary conditions.

The non-slip condition must be satisfied on the trumpet walls:

$$\nabla\tilde{P}\cdot\hat{n}\,\Big|_{\partial\Omega} = \vec{0}. \tag{23}$$

The surface describing the trumpet wall can be taken as a function of the parameters s and α ($\mathfrak{S} = f(s,\alpha)$). The radius ($r$) is a function of s only. Therefore, the surface is described as

$$\vec{\mathfrak{S}} = R(s)\hat{e}_r + \vec{C}(s). \tag{24}$$

The tangent plane is spanned by vector (25) and vector (26):

$$\vec{u} = \frac{d\vec{\mathfrak{S}}}{d\alpha} = \frac{dR\hat{e}_r}{d\alpha} + \frac{d\vec{C}(s)}{d\alpha} = R\hat{e}_\alpha, \tag{25}$$

$$\vec{w} = \frac{d\vec{\mathfrak{S}}}{ds} = \frac{dR\hat{e}_r}{ds} + \frac{d\vec{C}(s)}{ds} = R_s\hat{e}_r + (1 - R\kappa cos(\alpha))\hat{e}_s. \tag{26}$$

The normal vector to the surface is obtained as the cross product of the vectors $\vec{u}$ and $\vec{w}$:

$$\hat{n} = \vec{u}\times\vec{w} = RR_s\hat{e}_s - Rh_s\hat{e}_r. \tag{27}$$

The gradient in the helicoidal system is

$$\nabla\tilde{P} = \frac{1}{h_s}\tilde{P}_s\hat{e}_s + \tilde{P}_r\hat{e}_r + \frac{1}{R}\tilde{P}_\alpha. \tag{28}$$

The boundary condition on the walls of the trumpet:

$$\nabla\tilde{P}\cdot\hat{n} = \frac{R_s}{h_s^2}\tilde{P}_s - \tilde{P}_r = 0, \tag{29}$$

$$R_s\tilde{P}_s = \tilde{P}_r h_s^2. \tag{30}$$

In the nozzle:

$$\tilde{P}|_{s=0} = P_{max}(t). \tag{31}$$

At the bell:

$$\tilde{P}|_{s=L} = 0, \tag{32}$$

and according to the characteristic scales

$$\varepsilon^2 \frac{dR^*}{d\zeta}\frac{d\tilde{P}}{d\zeta} = \frac{d\tilde{P}}{d\varrho}h_s^2, \tag{33}$$

with $h_s^2 = 1 - \varepsilon\rho\varkappa cos(\alpha+\phi) + \varepsilon^2\rho^2\varkappa^2 cos^2(\alpha+\phi)$.

We propose an asymptotic expansion of $\tilde{P}$ in orders of ε

$$\tilde{P} = \tilde{P}_0 + \varepsilon\tilde{P}_1 + \varepsilon^2\tilde{P}_2 + \varepsilon^3\tilde{P}_3 + \ldots \tag{34}$$

Introducing the expansion (Equation (34)) into the wave equation and arranging in powers of ε we get

Order ε^0:

$$\frac{\partial^2\tilde{P}_0}{\partial\varrho^2} + \frac{1}{\varrho^2}\frac{\partial^2\tilde{P}_0}{\partial\alpha^2} + \frac{1}{\varrho}\frac{\partial\tilde{P}_0}{\partial\varrho} = 0, \tag{35}$$

Order ε:

$$\begin{aligned} &\frac{\partial^2\tilde{P}_1}{\partial\varrho^2} + \frac{1}{\varrho^2}\frac{\partial^2\tilde{P}_1}{\partial\alpha^2} + \frac{1}{\varrho}\frac{\partial\tilde{P}_1}{\partial\varrho} \\ &+\left(\frac{\varkappa\sin(\alpha+\phi)}{\varrho\hat{R}}\frac{\partial\tilde{P}_0}{\partial\alpha} - \frac{\varkappa\cos(\alpha+\phi)}{\hat{R}}\frac{\partial\tilde{P}_0}{\partial\varrho}\right) = 0, \end{aligned} \tag{36}$$

and order ε^2:

$$\begin{aligned} &\frac{\partial^2\tilde{P}_2}{\partial\varrho^2} + \frac{1}{\varrho^2}\frac{\partial^2\tilde{P}_2}{\partial\alpha^2} + \frac{1}{\varrho}\frac{\partial\tilde{P}_2}{\partial\varrho} \\ &+\left(\frac{\varkappa\sin(\alpha+\phi)}{\varrho\hat{R}}\frac{\partial\tilde{P}_1}{\partial\alpha} - \frac{\varkappa\cos(\alpha+\phi)}{\hat{R}}\frac{\partial\tilde{P}_1}{\partial\varrho}\right) \\ &+\left(\frac{1}{\hat{R}}\frac{\partial}{\partial\zeta}\left(\frac{1}{\hat{R}}\frac{\partial\tilde{P}_0}{\partial\zeta}\right) - \frac{\partial^2\tilde{P}_0}{\partial t^{*2}}\right) = 0. \end{aligned} \tag{37}$$

When expanding $\tilde{P}$ from Equation (30) in orders of ε we get the boundary conditions in the wall for each order:

$$\frac{d\tilde{P}_0}{d\varrho} = 0, \tag{38}$$

$$\frac{d\tilde{P}_1}{d\varrho} = 0, \tag{39}$$

$$\varkappa\varrho\cos(\alpha+\phi)\frac{d\tilde{P}_2}{d\varrho} = \frac{dR^*}{d\zeta}\frac{d\tilde{P}_0}{d\zeta}. \tag{40}$$

This system of equations with asymptotic expansion is analogous to the system proposed by Webster [19]; therefore it reduces to

$$\frac{1}{A}\frac{d}{d\zeta}\left(A\frac{d\tilde{P}}{d\zeta}\right) + k^2\tilde{P} = 0, \tag{41}$$

where A is the cross-sectional area of the pipeline

$$\frac{d^2\tilde{P}}{d\zeta^2} + \frac{A_\zeta}{A}\frac{d\tilde{P}}{d\zeta} + k^2\tilde{P} = 0 \tag{42}$$

and $A_\zeta = \frac{dA}{d\zeta}$.

In this work we will take two approaches to the relation of the dimensionless radius and the coordinate ζ. One will be linear and the other exponential. This is used to contrast two extreme cases of growth in order to explore which one best models the morphology of a snail's shell (in the review process of the present paper additional information has been obtained which suggests that growth is linear).

We assume that ϱ is a function of ζ.

Linear Approach

We propose a linear relationship between ϱ and ζ:

$$\varrho = \eta\zeta + \varrho_0 \quad \therefore A = \hat{r}^2\pi\varrho^2, \quad A_\zeta = \hat{r}^2 2\pi\varrho\eta, \quad \eta + \varrho_0 = 1. \tag{43}$$

The differential Equation (42) reduces to

$$\frac{d^2\tilde{P}}{d\zeta^2} + \frac{2}{\zeta + \zeta_0}\frac{d\tilde{P}}{d\zeta} + k^2\tilde{P} = 0, \tag{44}$$

with $\zeta_0 = \varrho_0/\eta$ being the relationship that exists between the trumpet nozzle and the bell.

Incorporating the change of variable $\zeta' = \zeta + \zeta_0$:

$$\frac{d^2\tilde{P}}{d\zeta'^2} + \frac{2}{\zeta'}\frac{d\tilde{P}}{d\zeta'} + k^2\tilde{P} = 0. \tag{45}$$

Multiplying the Equation (45) by ζ'^2:

$$\zeta'^2\frac{d^2\tilde{P}}{d\zeta'^2} + 2\zeta'\frac{d\tilde{P}}{d\zeta'} + \zeta'^2 k^2\tilde{P} = 0. \tag{46}$$

Equation (46) is the spherical Bessel equation of order 0; its solutions are widely known.

The solution in the original variable:

$$\tilde{P} = B\frac{\sin((\zeta + \zeta_0)k)}{(\zeta + \zeta_0)k} + D\frac{\cos((\zeta + \zeta_0)k)}{(\zeta + \zeta_0)k}. \tag{47}$$

Using the properties of sines and cosines, Equation (47) is transformed to

$$\begin{aligned}\tilde{P} = &\frac{\sin(\zeta k)}{(\zeta + \zeta_0)k}\Big(B\cos(\zeta_0) - D\sin(\zeta_0)\Big) \\ &+\frac{\cos(\zeta k)}{(\zeta + \zeta_0)k}\Big(D\cos(\zeta_0) + B\sin(\zeta_0)\Big).\end{aligned} \tag{48}$$

Since B and D are constants for the moment, we can condense them as follows: $B' = B\cos(\zeta_0) - D\sin(\zeta_0)$ and $D' = D\cos(\zeta_0) + B\sin(\zeta_0)$. Rewriting Equation (48) in terms of the new constants,

$$\tilde{P} = B'\frac{\sin(\zeta k)}{(\zeta + \zeta_0)k} + D'\frac{\cos(\zeta k)}{(\zeta + \zeta_0)k}. \tag{49}$$

Through the pressure boundary conditions

$$\tilde{P}|_{\zeta=1} = B'\frac{\sin(k)}{(1 + \zeta_0)k} + D'\frac{\cos(k)}{(1 + \zeta_0)k} = 0, \tag{50}$$

$\zeta_0 \neq 0$,

$$\tilde{P}|_{\zeta=0} = B'\frac{\sin(0)}{\zeta_0 k} + D'\frac{\cos(0)}{\zeta_0 k} = P_{max}, \tag{51}$$

and therefore

$$D' = -B'\tan(k). \tag{52}$$

We know that at the point $\zeta = 0$ the pressure must be maximal, since along the way the flow expands due to the incremental change in section.

We rewrite the boundary condition

$$\frac{d\tilde{P}}{d\zeta}|_{\zeta=0} = B'\frac{\cos(0)}{\zeta_0} - B'\frac{\sin(0)}{\zeta_0^2 k} - D'\frac{\cos(0)}{\zeta_0^2 k} - D'\frac{\sin(0)}{\zeta_0^2} = 0, \tag{53}$$

simplifying

$$D' = B'k\zeta_0. \tag{54}$$

Using Equations (52) and (54) we can get an equation only for the wave number

$$tan(k) = -k\zeta_0, \quad tan(k) + k\zeta_0 = 0. \tag{55}$$

In such a way there are multiple wave numbers, all satisfying Equation (55). The solution for the space part is

$$\tilde{P} = \sum_{n=1}^{\infty} B'_n \left(\frac{\sin(k_n\zeta)}{k_n(\zeta+\zeta_0)} - \tan(k_n)\frac{\cos(k_n\zeta)}{k_n(\zeta+\zeta_0)} \right). \tag{56}$$

In the special case when $\zeta_0 = 0$, the function $\cos(\zeta k)/\zeta k$ is not admissible since it is not defined in the domain specifically when $\zeta = 0$,

$$\tilde{P}|_{\zeta=0} = B'\frac{\sin(\zeta)}{\zeta} + D'\frac{\cos(\zeta)}{\zeta} = P_{max}, \quad \therefore D' = 0, \tag{57}$$

$$\tilde{P}|_{\zeta=1} = B'\frac{\sin(k)}{k} = 0 \quad \therefore \quad \sin(k) = 0, k_n = n\pi, n \in \mathbb{N}. \tag{58}$$

$$K_n = \frac{k_n}{L}. \tag{59}$$

Finally for this specific case the spatial solution of the pressure is

$$\tilde{P} = \sum_{n=1}^{\infty} B_n \frac{\sin(k_n\zeta)}{k_n\zeta}. \tag{60}$$

For the second case exponential growth is proposed:

$$\varrho = \varrho_0 e^{\beta\zeta} \quad \therefore A = \hat{r}^2\pi\varrho^2, \quad A_\zeta = \hat{r}^2 2\pi\varrho^2\beta, \quad \beta = \ln\left(\frac{1}{\varrho_0}\right). \tag{61}$$

The differential Equation (42) is reduced to

$$\frac{d^2\tilde{P}}{d\zeta^2} + 2\beta\frac{d\tilde{P}}{d\zeta} + k^2\tilde{P} = 0. \tag{62}$$

The equation is solved via the Cauchy differential polynomial

$$\lambda^2 + 2\beta\lambda + \kappa^2 = 0, \tag{63}$$

$$\lambda = -\beta \pm \sqrt{\beta^2 - \kappa^2}. \tag{64}$$

Due to the oscillating nature of the waves, it is assumed

$$\tilde{P} = B'_1 e^{-\beta\zeta + i\phi\zeta} + B'_2 e^{-\beta\zeta - i\phi\zeta}. \tag{65}$$

Using Euler's identity

$$\tilde{P} = e^{-\beta\zeta}\Big(B_1 cos(\phi\zeta) + B_2 sen(\phi\zeta)\Big) \tag{66}$$

satisfying boundary conditions

$$\tilde{P}|_{\zeta=1} = e^{-\beta}\Big(B_1 cos(\phi) + B_2 sen(\phi)\Big) = 0, \tag{67}$$

$$B_1 cos(\phi) + B_2 sen(\phi) = 0, \tag{68}$$

$$\begin{aligned} \frac{d\tilde{P}}{d\zeta} &= -\beta e^{-\beta\zeta}(B_1 cos(\phi\zeta) + B_2 sen(\phi\zeta)\Big) \\ &+\phi e^{-\beta\zeta}(-B_1 sen(\phi\zeta) + B_2 cos(\phi\zeta)\Big), \end{aligned} \tag{69}$$

$$\frac{d\tilde{P}}{d\zeta}|_{\zeta=0} = -\beta B_1 + \phi B_2 = 0, \tag{70}$$

$$B_2 = \frac{\beta}{\phi} B_1. \tag{71}$$

Replacing (71) in (68) we get

$$B_1 cos(\phi) + \frac{\beta}{\phi} B_1 sen(\phi) = 0, \tag{72}$$

$$\frac{\phi}{\beta} + \tan(\phi) = 0, \tag{73}$$

$$k = \sqrt{\phi^2 + \beta^2}. \tag{74}$$

Due to fact that Webster's equation comes from a separation of variables of the wave equation, the separation constant relates the wave number and the angular frequency via the speed of sound (c_0). Therefore a relationship can be obtained with the overtones of the instrument

$$\omega_n = \frac{k_n c_0}{L} \tag{75}$$

and

$$\omega_n = 2\pi f_n. \tag{76}$$

Both overtones are presented in terms of wave numbers, where ω_n is the angular frequency, k_n is the dimensionless wave number and f_n is the frequency of the overtone:

$$f = \frac{k_n c_0}{2\pi L}, n \in \mathbb{N}. \tag{77}$$

Finally, we arrive at the main conclusion for the wave number; we obtain two solutions: linear case:

$$tan(k) + k\zeta_0 = 0, \tag{78}$$

and exponential case:

$$\frac{\sqrt{\beta^2 - k^2}}{\beta} + \tan(\sqrt{\beta^2 - k^2}) = 0. \tag{79}$$

The presented analytical model does not consider fluid–structure interactions; in particular, the effect of the shell material is not taken into account. The curvature is not present explicitly in the solution due to the fact that in the asymptotic expansion its contribution only appears in higher order terms.

4. Experimental Data

Recordings of different pre-Hispanic Maya trumpets have been obtained. For the acoustic study of archaeological sound instruments, an experimental setup was implemented, consisting of a mobile soundproof chamber (to maintain the same recording conditions; Figures 5 and 6 show the soundproof chamber and a diagram), an ECM 800 microphone, an HP laptop, cables, a sound level meter, a decibel meter, Digi 002 interfaces (with 4 analog channels and 2 digital channels), and a Tascam US-122. The soundproof chamber is suspended and walls are covered with acoustically insulating material. The level meter and decibel meter are built to verify the recording conditions since it is desirable to know how much the decibels decrease in the booth compared to the outside so that they are as homogeneous as possible for each occasion in which the instruments are played. Since this is a mobile chamber, every time it is assembled, it is necessary to verify that standard conditions are satisfied.

Figure 5. Mobile soundproof chamber; due to museum regulations the shells cannot be taken out.

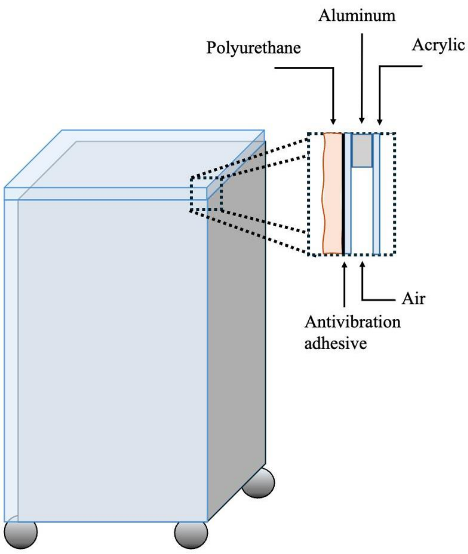

Figure 6. Mobile soundproof chamber diagram. The room is a parallelepiped with a base of 104 cm by 104 cm and a height of 190 cm. The exterior walls consist of a 5 mm acrylic panel and a 2-inch-thick aluminum beam structure, with air gaps between the acrylic panels for insulation. The interior walls are made of 2-inch-thick, low-density, acoustic-grade PU.

Once the experimental device was set up to obtain the sound emitted by the trumpets, the performer (Roberto Carbajal) performed the different excitations inside the mobile soundproof chamber, and a team member outside the chamber recorded the signals using specialized recording software. The performer took an appropriate position to play each trumpet, trying to produce as many tones as possible. The performer, after some experimentation with the instrument and his expertise, plays the fundamental note, which is the frequency that sounds the loudest with the same input. So, with the experimental limitations we had (the instruments cannot be taken out for standard measurements), when the performer played a note far from the fundamental, the instrument produced a weak sound. The person outside recorded the sounds from within the chamber, which were then available for editing and analysis. The recordings were made in wave format with a sampling frequency of 44,100 Hz.

From the recordings, the acoustic pressure signal is stored over time as shown in Figure 7.

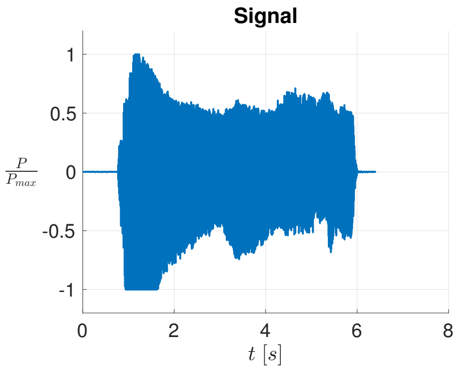

Figure 7. Normalized pressure (282,302 samples recorded at 44.1 kHz) signal of archaeological piece 10-342833.

The analysis is performed on six different archaeological pieces. Four pieces are snail sea shells (Figures 8–11), and two are ceramic trumpets (Figures 12 and 13) that resemble the shape of a snail shell.

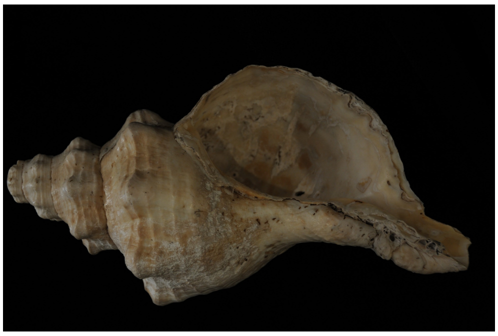

Figure 8. Instrument inventory number 10-342833, from a rescue excavation in Jaina, registered as MRA-00214, 584/76, p. 17. Photo by Andrés Alux Medina.

Figure 9. Instrument inventory number 10-412971, from Plazuelas, Guanajuato. Photo by Francisca Zalaquett.

Figure 10. Instrument inventory number 10-412970, from Plazuelas, Guanajuato. Photo by Francisca Zalaquett.

Figure 11. Instrument inventory number 10-621154, housed in the Maya Room of the National Museum of Anthropology, from Chichén Itzá, Yucatán, Late Postclassic period. Photo from the Digitalization Project, National Museum of Anthropology.

Figure 12. Ceramic "trumpet" in the form of a ceramic conch, inventory number 10-223524, housed in the Maya Room of the National Museum of Anthropology, Mexico, with a hole. Photo from the Digitalization Project, National Museum of Anthropology.

Figure 13. Ceramic "trumpet" in the form of a conch, inventory number 10-393463, housed in the Maya Room of the National Museum of Anthropology. Photo from the Digitalization Project, National Museum of Anthropology.

We chose a variety of aerophones to verify if there are features in common among snail shells and the ceramic pieces. In Table 1 we give details of the morphology of the aerophones.

Table 1. Morphological details of aerophones.

Piece #	Nozzle Diameter	Aperture Diameter	ζ_0	β
10-621154	4.22 mm	34.26 mm	0.140	2.094
10-223524	16.14 mm	106 mm	0.179	1.882
10-393463	5.84 mm	77.8 mm	0.081	2.589
10-342833	11.63 mm	119.97 mm	0.073	2.676
10-412970	9 mm	126.4 mm	0.076	2.642
10-412971	13.6 mm	129.690 mm	0.117	2.255

5. Results

Recordings of different Mesoamerican trumpets have been obtained. Through measurements, the theoretical harmonics (from the previously derived solutions) have been compared with those obtained experimentally from recordings. With the audio recordings and the Fourier transform we obtain the frequency spectrum as shown in Figure 14.

At first, the audio signal was obtained from a recording as shown in Figure 7. The main harmonics were obtained from the frequency spectrum as shown in Figure 14.

To compare the experimental and the theoretical data, it is necessary to measure the length of the path and the speed of sound, but these are variables susceptible to errors and are not so easy to measure (especially the path length due to the nature of helical trumpets). Therefore we decided to normalize the measurements of fundamental harmonics dividing them by the frequency of their fundamental (as explained in further detail below).

From experimental signals and using the Fourier transform it was possible to plot the frequency spectrum for each piece (as example Figure 14).

Each frequency spectrum was divided into segments (first five overtones) with a local maximum as the center of each segment.

We obtained the expected value for each overtone, with its respective standard deviation (Figure 15).

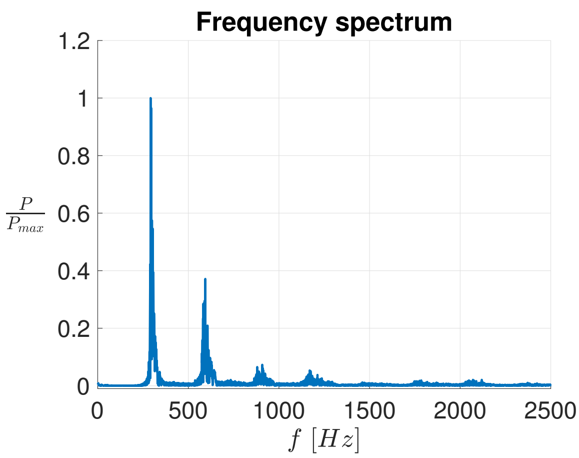

Figure 14. Frequency spectrum (141,152 points) of archaeological piece 10-342833.

Then each of the five expected values were normalized, dividing by the first overtone, giving a dimensionless frequency. We remark that the variations in the harmonics due to the temperature and humidity are negligible (maximum variations in the speed of sound due to temperature and humidity amount to at most 5%); they cancel after normalization.

https://doi.org/10.3390/acoustics8020023

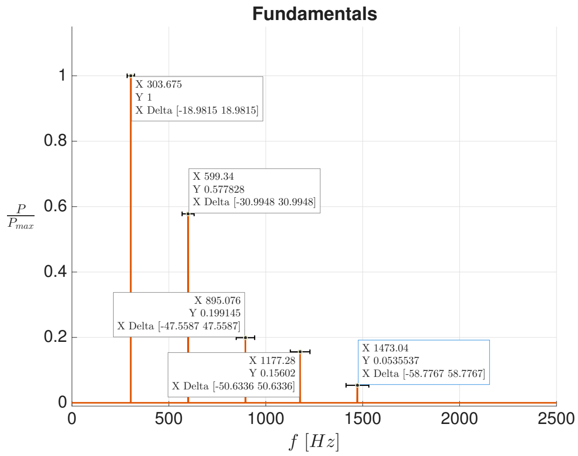

Figure 15. Fundamental and 4 overtones of the archaeological piece 10-342833. The error bar shows the standard deviation.

As a result, every frequency spectrum plot was turned into a graph with five dimensionless overtones and their standard deviations. The experimental data was compared to the linear and exponential mathematical models developed in previous sections, where Equations (78) and (79) were obtained. The equations were solved for k with a numerical method. The following Figures 16–21 show this comparison with the experimental data for all the previously mentioned pieces.

Experimental results are given below.

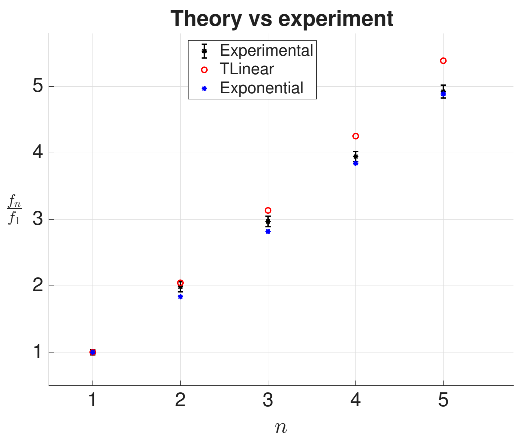

Figure 16. Normalized overtones showing better exponential fitting, obtained from the shell-like ceramic piece 10-223524.

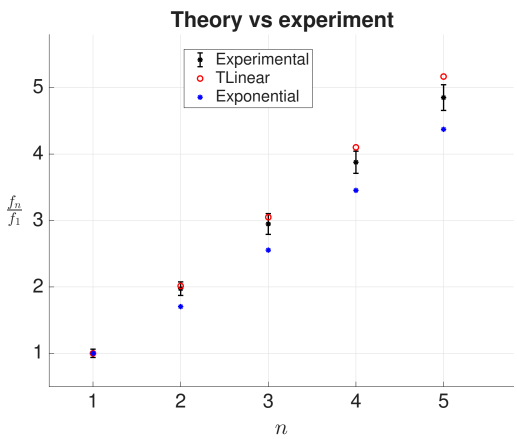

Figure 17. Normalized overtones showing better linear fitting, obtained from the shell piece 10-342833.

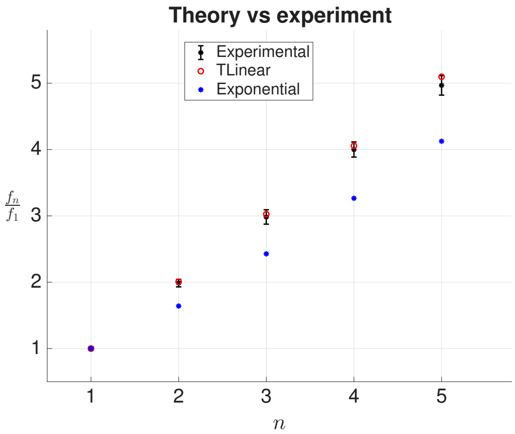

Figure 18. Normalized overtones showing better linear fitting, obtained from the ceramic shell piece 10-393463.

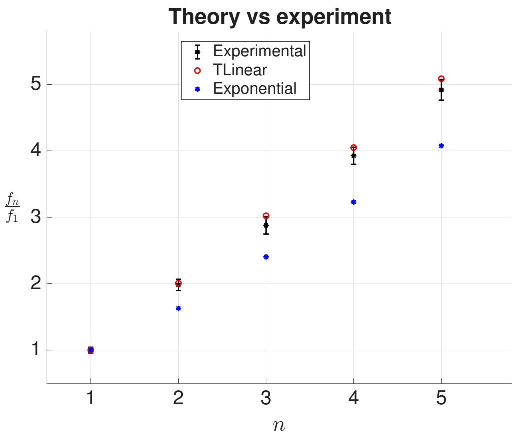

Figure 19. Normalized overtones showing better linear fitting, obtained from the shell piece 10-412970.

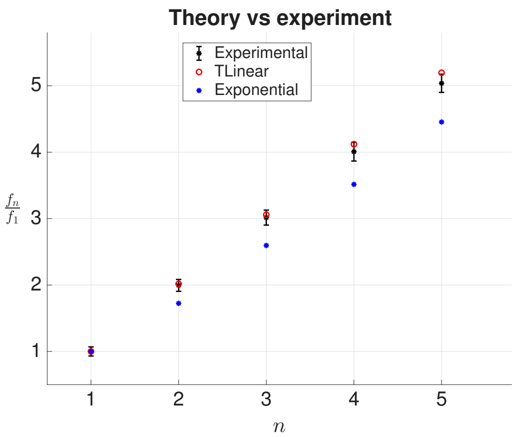

Figure 20. Normalized overtones showing better linear fitting, obtained from the shell piece 10-412971.

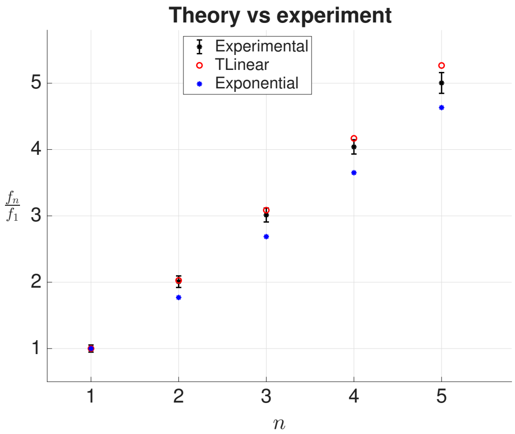

Figure 21. Normalized overtones showing better linear fitting, obtained from the shell piece 10-621154.

6. Conclusions

A mathematical model was developed to describe the geometry of the snail shell in terms of a moving curve with three coordinates, which allowed us to write a differential equation that describes the motion of waves within a snail shell in terms of its geometry. This equation was simplified to 1-D, considering a variable transversal area, and an analytical solution was obtained that predicts the overtones of any snail shell based on its radial growth as a function of its arc length. Our solutions are equivalent to a right cone. It should be emphasized that the entire mathematical process and coordinate system were used to justify using this approximation, as well as to understand its limitations and the relationship of the small factors to be considered. In Rienstra's work [21], the extension to any system of concurved and twisted pipes is not obvious. Linear and exponential radial growth were assumed, and these mathematically obtained overtones were compared with those recorded experimentally.

In piece 10-342833, belonging to a Pleuroploca gigantea snail seashell recovered from Campeche (Figure 10), it was observed that the experimental overtones matched the linear model. In pieces 10-412 970 and 10-412 971 (Figures 7 and 12), both from a different collection than the previous one (but from the same species), a good agreement was also found between the linear model and the experimentally recorded overtones. This suggests that for this species, the growth of the snail shell's radius maintains a linear relationship with respect to the length of its arch, thus providing overtones comparable with the solution of Equation (78).

In piece 10-621 154 (a different species than the previous ones), the same as before was found between the linear model and the experimentally recorded overtones (although, as observed in Figure 13, this snail shell has a less pronounced curvature and is smaller). Therefore, it was found that Equation (78) can once again be used satisfactorily to predict its acoustics.

For piece 10-393 463 (a ceramic piece similar in morphology to Pleuroploca gigantea shells, as seen in Figure 9), the experimentally obtained overtones were (as with real shells) equal to those predicted by the linear model.

For piece 10-223 524 (a ceramic piece), the experimentally obtained overtones were closer to the exponential model (Equation (79)). This is explained by its distant morphology (with a pronounced width) from real shells, as seen in Figure 8, thus demonstrating that its acoustics do not reflect those of a real shell.

Finally, DEs have proven to be useful for approximating the overtones and morphology of helical systems with archaeological applications as long as three parameters are known—the diameter of the nozzle, the diameter of the aperture and the total arc length—regardless of the conditions and state of conservation of the original piece; that is, it is applicable even for priceless pieces, those of extreme fragility and/or those that are permanently damaged (product of symbolic liberation rituals as described earlier and other causes). By a geometric characterization from tomographic imaging (indirect measurements) it is possible to calculate path lengths and from DE resolutions recreate the original sounds, providing deeper insights into the cultural and acoustic dimensions of ethnomusicology.

Author Contributions: P.P. and F.Z. designed and directed the project; F.Z. performed the experiments and obtained the experimental resources; M.-A.R.-T. wrote the final draft and developed the theoretical and numerical framework; M.S.-V. and P.P. supervised the mathemathical modelling. All authors have read and agreed to the published version of the manuscript.

Funding: This research received no external funding.

Institutional Review Board Statement: Ethical approval was not sought for the present study because no human or living animal data obtained from experiments were used.

Data Availability Statement: The data that support the findings of this study are available from the corresponding author upon reasonable request.

Acknowledgments: We appreciate the support of CONAHCYT grant number 859082. Authors would like to thank the Instituto de Ingenieria. This work was carried out with the support of PAPIIT fund number IN403724, titled "Mayan Soundscapes. Diachronic Analysis of Their Instruments, Architecture, and Biological, Geographic, and Meteorological Elements That Form Part of Their Daily Life," from the Maya Studies Center, Institute of Philological Research at the National Autonomous University of Mexico.

Conflicts of Interest: The authors declare that they have no conflicts of interest.

References

1. Fritz, C.; Tosello, G.; Fleury, G.; Kasarherou, E.; Walter, P.; Duranthon, F.; Gaillard, P.; Tardieu, J. First record of the sound produced by the oldest Upper Paleolithic seashell horn. *Sci. Adv.* **2021**, *7*, eabe9510. [CrossRef] [PubMed]
2. Dubreuil, L.; Ovadia, A.; Shahack-Gross, R.; Grosman, L. Evidence of ritual breakage of a ground stone tool at the Late Natufian site of Hilazon Tachtit cave (12,000 years ago). *PLoS ONE* **2019**, *14*, e0223370. [CrossRef] [PubMed]
3. Armiñana, G.; Fimia, D.; Iannacone, J. *Catálogo Ilustrado de los Moluscos Dulceacuícolas de Cuba Importancia Médico-Veterinaria*; José Iannacone Oliver: Lima, Peru, 2021.
4. del Río, J.C.; Chiappara, S.M. *Moluscos Marinos Miocenos de la Argentina y del Uruguay*; Academia de Ciencias Exactas, Físicas y Naturales: Madrid, España, 1998.
5. Vilenski, G.; Rienstra, S. Acoustic modes in a ducted shear flow. In Proceedings of the 11th AIAA/CEAS Aeroacoustics Conference, Monterey, CA, USA, 23–25 May 2005; p. 3024.
6. Böhnke, F.; Arnold, W. 3D-finite element modelof the human cochlea including fluid-structure couplings. *ORL* **1999**, *61*, 305–310. [CrossRef] [PubMed]
7. Bonfiglio, P.; Pompoli, F. A numerical approach for the analysis of car snail horn performance. *Noise Control Eng. J.* **2017**, *65*, 147–157. [CrossRef]
8. Zhang, M.X.; Sun, Q.Y.; Zhang, B.Y. Analysis for the Sound Channel Performance of the Snail Shell-like Horn. *J. Harbin Univ. Sci. Technol.* **2011**, *16*, 3.
9. Rath, S.K.; Naik, P. A study on acoustics of conch shell. *Curr. Sci.* **2009**, *97*, 521–528.
10. Morteza Pouraghdam, R. Numerical Analysis and Experiments on the Acoustics of Conch Shells Modelled as Spiral Cavities. Ph.D. Thesis, Concordia University, Montreal, QC, Canada, 2016.
11. Rath, S.K.; Naik, P. On acoustic theory of conch shell. *Curr. Sci.* **2010**, *99*, 790–795.
12. Thompson, D.W. *On Growth and Form*; Cambridge University Press: Cambridge, UK, 1917.
13. Dean, W. XVI. Note on the motion of fluid in a curved pipe. *London Edinburgh Dublin Philos. Mag. J. Sci.* **1927**, *4*, 208–223. [CrossRef]
14. Dean, W. LXXII. The stream-line motion of fluid in a curved pipe (Second paper). *London Edinburgh Dublin Philos. Mag. J. Sci.* **1928**, *5*, 673–695. [CrossRef]
15. Germano, M. The Dean equations extended to a helical pipe flow. *J. Fluid Mech.* **1989**, *203*, 289–305. [CrossRef]
16. Germano, M. On the effect of torsion on a helical pipe flow. *J. Fluid Mech.* **1982**, *125*, 1–8. [CrossRef]
17. Vasudevaiah, M.; Patturaj, R. Effect of torsion in a helical pipe flow. *Int. J. Math. Math. Sci.* **1994**, *17*, 553–560. [CrossRef]

18. do Carmo, M.P. *Differential Geometry of Curves and Surfaces*; Prentice-Hall, Inc.: Englewood Cliffs, NJ, USA, 2016; Volume 510.
19. Webster, A.G. Acoustical impedance and the theory of horns and of the phonograph. *Proc. Natl. Acad. Sci. USA* **1919**, *5*, 275. [CrossRef] [PubMed]
20. Rienstra, S.W.; Hirschberg, A. An introduction to acoustics. *Tech. Univ. Eindh.* **2004**, *18*, 372.
21. Rienstra, S.W. Webster's horn equation revisited. *SIAM J. Appl. Math.* **2005**, *65*, 1981–2004. [CrossRef]

https://doi.org/10.3390/acoustics8020023